Pergamon

Mathl. Comput. Modelling Vol. 19, No. 2, pp. 61–77, 1994

0895-7177/94 $6.00 + 0.00

0895-7177(94)E0016-G

An Optimization Procedure for Maximizing the Energy Absorption Capability of Composite Shells

J. M. FERREIRA AND A. CHATTOPADHYAY
Department of Mechanical and Aerospace Engineering
Arizona State University, Tempe, AZ 85287, U.S.A.

(Received June 1993; revised and accepted September 1993)

Abstract—Composite cylindrical shells are being used more extensively for structural applications in both rotary- and fixed-wing aircraft where low weight and high strength are important design issues. This paper addresses the energy absorption capability of such shells, under axial compressive loading. A design optimization procedure is developed to improve the energy absorption by maximizing the buckling and postbuckling characteristics of the shells. The sensitivity of both geometric and material properties is investigated by studying thin-walled shells of several thicknesses, made of different types of orthotropic laminates. Constraints are imposed on the longitudinal, normal, and in-plane shear stresses of each ply by utilizing a failure criteria. Design variables include shell diameter and ply orientations. The optimization is performed using the nonlinear programming method of feasible directions. A two-point exponential approximation is also used to reduce computational effort. Results are presented for Graphite/Epoxy, Glass/Epoxy, and Kevlar/Epoxy composite cylindrical shells with symmetric ply arrangements.

Keywords—Energy absorption, Optimization, Composite shell, Buckling and postbuckling.

NOMENCLATURE

a_{ij}, b_{ij}, d_{ij}	compliance matrix elements
$g_j(\Phi)$	j^{th} constraint function
k_x, k_y, k_{xy}	laminate curvatures, in^{-1}
$\mathbf{k}$	laminate curvature vector, in^{-1}
l_x, l_y	axial and circumferential half-wavelengths of radial displacements
m	number of buckle half-waves in axial direction of the shell
n	number of buckle waves in circumferential direction of the shell
$\mathbf{s}$	off-axis stress vector, lb/in^2
t	total shell wall thickness, in
u, v, w	axial, circumferential, and radial displacements of shell wall
$\bar{u}, \bar{v}, \bar{w}$	amplitudes of buckling displacement functions
u^0, v^0	axial and circumferential displacements of shell wall mid-plane
$w_0, \ldots, w_4$	radial deflection parameters
x, y, z	axial, circumferential, and radial coordinates on shell reference surface (global-axes)
A_{ij}	extensional stiffness matrix element, lb/in
D_{ij}	bending stiffness matrix element, lb-in
$\mathbf{A}$	extensional stiffness matrix, lb/in
$\mathbf{B}$	coupling stiffness matrix, lb-in/in
$\mathbf{D}$	bending stiffness matrix, lb-in
E_1	longitudinal elastic modulus of composite, lb/in^2
E_2	transverse elastic modulus of composite, lb/in^2
$F(\Phi)$	objective function
G_{12}	in-plane shear elastic modulus of composite, lb/in^2

This research is sponsored in part by grants from the National Science Foundation, Grant Number MSS-9209961, and the Army Research Office, Grant Number DAAHOH-93-G-0043.

L	length of cylindrical shell, in
M_x, M_y, M_{xy}	in-plane moments on laminate, lb-in/in
$\mathbf{M}$	resultant moment vector, lb-in/in
N_x, N_y, N_{xy}	in-plane forces on laminate, lb/in
$\bar{N}_x$	applied axial force, lb/in
N_x	buckling load, lb/in
$N_{x_{cr}}$	critical buckling load, lb/in
$\mathbf{N}$	resultant force vector, lb/in
NCON	number of constraints
NDV	number of design variables
$\bar{\mathbf{Q}}$	off-axis stiffness matrix, lb/in^2
R	mean radius of cylindrical shell, in
$\mathbf{T}$	transformation matrix
V_F	volume fraction of fibers in composite, percent
$\varepsilon_x^0, \varepsilon_y^0, \gamma_{xy}^0$	laminate mid-plane strains
$\boldsymbol{\varepsilon}^0$	laminate mid-plane strain vector
$\bar{\varepsilon}$	average end shortening, in/in
ν_{12}, ν_{21}	major and minor Poisson ratios
$\phi(x, y)$	Airy stress function
ϕ_i	i^{th} design variable
Φ	design variable vector
$\mu = l_y/l_x$	wavelength ratio parameter
Π	total potential energy function
ρ	density of composite, lb/in^3
σ_{1T}	longitudinal tensile strength, lb/in^2
σ_{1C}	longitudinal compressive strength, lb/in^2
σ_{2T}	transverse tensile strength, lb/in^2
σ_{2C}	transverse compressive strength, lb/in^2
σ_{12S}	in-plane shear strength, lb/in^2
σ_T	tensile strength bound, lb/in^2
σ_C	compressive strength bound, lb/in^2
$\bar{\sigma}$	average axial compressive load, lb/in
$\boldsymbol{\sigma}$	material-axis stress vector, lb/in^2
θ	fiber orientation angle, degrees
Subscripts	
1, 2	longitudinal and transverse fiber directions
C	compressive
L	lower bound
T	tensile
U	upper bound

INTRODUCTION

The role of composite materials in structural applications has extensively increased over the past decade due to their reduced-weight and high-strength capabilities. Composites have found widespread use in aerospace and automotive vehicles. Therefore, passenger survivability, in the event of an accident, can be greatly influenced by the performance of the structural composite components. To help assure passenger safety and survivability in accidents, the military and the government have been setting crashworthy standards that newly developed land and air vehicles must meet. In order to better adhere to crashworthy design requirements, it is necessary to maximize the amount of energy that vehicle structural components can absorb.

Various investigations have been performed over the past several years to understand post-failure deformation and the energy absorption capabilities of composites. Research has been primarily focused on composite beams [1–3] and tubes [2,4–13]. In these investigations, parametric studies were performed on I-beams and short tubes with small radii to examine the effect of material properties such as modulus, geometric properties such as ply orientation and stacking sequence, and loading rate on energy absorption. The results are often conflicting in nature. The experiments are also expensive to conduct. Therefore, although a large database in information of energy absorption of composite specimens with various cross sections is available, it is essential to perform analytical investigations of the mechanism of energy absorption.

A commonly used structural component found in vehicles is the shell. Specifically, the shell of revolution or cylindrical shell has found the most wide spread use in the design of vehicles. Since shells are ideal for carrying many different types of loads, composites can be used to optimize its structural performance to best suit a particular loading configuration. For crashworthy applications, it is also important to improve the energy absorbing capabilities of the shell. This requires the determination of optimum material and geometric characteristics for efficient buckling and postbuckling deformations.

In this paper, a structural optimization procedure is proposed for the design of composite cylindrical shells for improved pre- and postfailure performance. Although a significant amount

of work has been done in the area of structural optimization, a great majority of this work has been limited to isotropic materials where the design variables are generally size, shape, and topology. With the emergence of fiber-reinforced composites, it is now possible to consider design parameters related to material properties, either at the ply or at the laminate level. Due to the importance of the problem, there has been some effort towards using structural optimization procedures for design with composites in recent years [14–19]. Typically structures were designed for minimum weight, using ply orientations, thicknesses, and sometimes number of plies as design variables. Vanderplaats and Weisshaar [18] addressed the optimization of membrane panels, both unstiffened and stiffened, with constraints on strains and frequencies. The design of an aeroelastically tailored wing was also discussed in this paper. Pederson [17] investigated the problems of optimal ply orientation of a uniform cantilever beam and a bending-loaded knee. He also addressed the problem of optimal shape design using orthotropic material. Gurdal and Haftka [15] used integer programming and techniques such as genetic algorithms to address the problem of optimum ply stacking sequences. The optimization of axially compressed composite cylindrical shells for minimum weight was addressed by Zimmermann [19], where the ply orientations were used as design variables, and constraints were placed on the buckling load. This technique posed certain difficulties, since the objective function and the constraints were not functions of the design variables used. Onada [16] and Fukunaga and Vanderplaats [14] used lamination parameters to investigate the buckling loads of cylinders under axial and combined loadings. Most recently, Ferreira, Chattopadhyay and Pringnitz [20] addressed the problem of reducing interlaminar stresses in composite plates using a multiobjective optimization technique. The interlaminar stress magnitudes at each ply interface were used as the objective functions, and constraints were placed on the ply stresses. Ply orientations were used as design variables.

Although a considerable effort has been devoted in improving prefailure performance of a structural member, postfailure performance and the problem of improving energy absorption characteristics using formal optimization procedures has not been addressed in much depth. To date, very little published research is available in this area. Lust [21] presented a structural design optimization methodology for automobiles, considering design criteria associated with both linear elastic and crashworthiness (nonlinear) conditions. By simultaneously using both elastic and crashworthy criteria, more mass efficient structural designs were obtained. However, in the modeling of the postcritical behavior, a scaling factor was utilized to approximate the nonlinear crashworthy constraints. Bolukbasi [22] developed a preliminary design optimization methodology for possible rotorcraft applications. The procedure minimized the system weight of a helicopter while maintaining a specific level of crash protection. Crash response analysis tools and parametric subsystem weight analyses were employed in the optimization.

The goal of this research is to use formal design optimization procedures to maximize the energy absorbing capability of axially compressed composite cylindrical shells with constraints on the individual ply stresses and the critical buckling load. Both the pre- and postfailure responses are modeled analytically. Additionally, a sensitivity analysis is performed to examine energy absorption with respect to material constitutive properties and geometry.

PROBLEM DESCRIPTION

The energy absorption capability is quantified by the area under the force-deflection curve (Figure 1) and is used as an objective function. Design variables include individual ply orientations. Constraints are imposed on the in-plane material-axis stresses of each ply and the critical buckling load. A structural analysis procedure, based on laminate and shell theory, is used for determining the buckling and postbuckling characteristics. The nonlinear programming method of feasible directions combined with a two-point exponential approximation procedure is used for the optimization. A study is also conducted to examine the sensitivity of energy absorption with

respect to material constitutive properties. Therefore, cylindrical shells made of Gr/Ep, Gl/Ep, and K/Ep with a varying number of symmetric lay-ups are investigated.

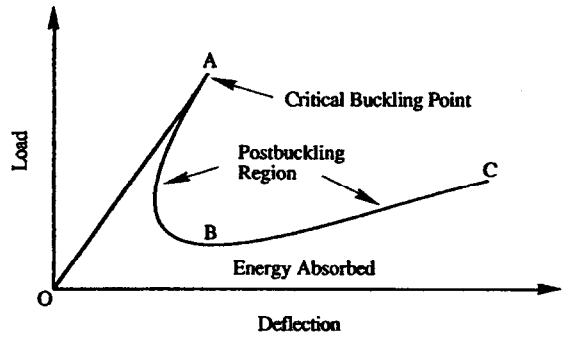

Figure 1. Typical load-deflection graph of an axially compressed cylindrical shell.

STRUCTURAL MODEL

A geometric illustration of a typical composite cylindrical shell and laminate considered in this study is presented in Figures 2 and 3. The initial or reference shells all have a length $L = 50$ inches, an inner radius $R = 10$ inches ($L/R = 5$), and alternating ply orientations of $\pm 30°$. For example, a 6-ply shell has a reference orientation of $[+30/-30/+30]_S$. A $\pm 30°$ lay-up scheme is chosen since it represents a typical configuration used in industry. The total number of plies used to make up the wall thickness, t, is varied in each specimen. The plies are numbered starting from 1 through to the final ply in the laminate, with the first ply being the outer most one (Figure 2). A representative value of 0.01 inch is used for the thickness of each ply.

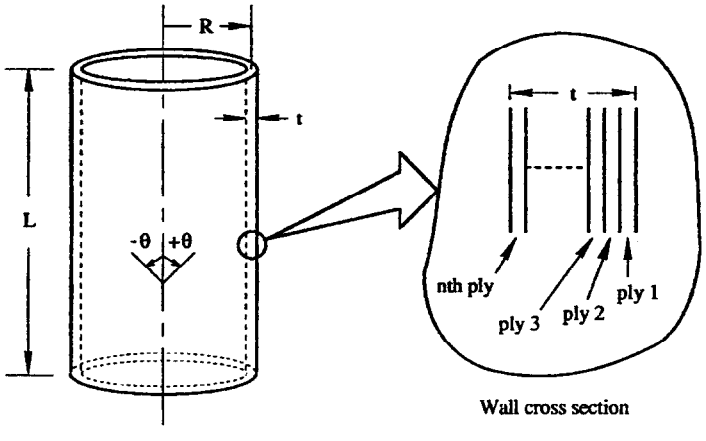

Figure 2. Composite cylindrical shell geometry and notation.

A global orthogonal curvilinear coordinate system for the shell and the laminate geometry is shown in Figure 3. The axial, circumferential, and radial coordinates are denoted x, y, and z, respectively, and the associated displacements are denoted u, v, and w. The material-axis coordinate system of the composites, denoted 1 and 2, is also shown in Figure 3, where 1 corresponds to the direction parallel to the ply fibers and 2 corresponds to the direction transverse to the ply fibers. The local coordinate system is related to the global through the angle θ.

A total of 15 cylindrical shells made of Graphite/Epoxy (Gr/Ep), Glass/Epoxy (Gl/Ep), and Kevlar/Epoxy (K/Ep) with 2, 4, 6, 8, and 10 ply symmetric orthotropic construction are investigated. The constituent material properties of the shells analyzed are presented in Table 1 [23].

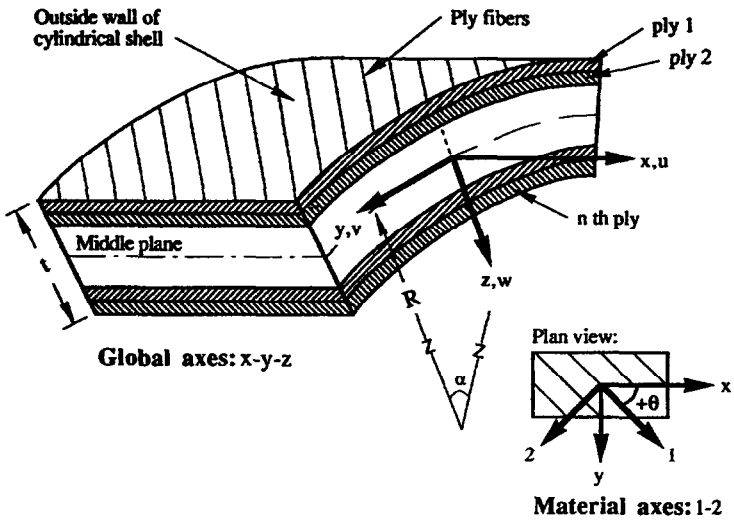

Figure 3. Axis orientation and geometric representation of laminates.

Table 1. Composite material properties.

	Gr/Ep	Gl/Ep	K/Ep
E_1 (psi)	20,000,000	8,300,000	10,000,000
E_2 (psi)	1,300,000	3,000,000	700,000
G_{12} (psi)	1,000,000	900,000	300,000
ν_{12}	0.3	0.26	0.34
σ_{1T} (psi)	210,000	289,000	210,000
σ_{1C} (psi)	210,000	170,000	50,000
σ_{2T} (psi)	7,500	11,000	6,000
σ_{2C} (psi)	30,000	29,000	10,000
σ_{12} (psi)	14,000	9,000	7,000
ρ (lb/in^3)	0.055	0.07	0.05
V_F (%)	67	67	60

ANALYSIS AND OPTIMIZATION

In this section, a brief description of the structural analysis procedure is presented, followed by a description of the formulation of the optimization problem. The implementation of the optimization procedure is described thereafter.

Laminate Analysis

The individual material-axis ply stresses of the orthotropic composite plates are analyzed using classical laminate theory [23]. The constitutive relations, relating ply strains and curvatures to the resultant forces and moments, are as follows:

$$\mathbf{N} = \mathbf{A}\,\varepsilon^0 + \mathbf{B}\,\mathbf{k}, \tag{1}$$

$$\mathbf{M} = \mathbf{B}\,\varepsilon^0 + \mathbf{D}\,\mathbf{k}, \tag{2}$$

where the only nonzero element in the matrix $\mathbf{N}$ is N_x (the axial compressive load). When a laminate is symmetric, the terms in the coupling stiffness matrix $\mathbf{B}$ are zero and the constitutive relation decouples. In the absence of moments, the curvature values are also zero.

The constitutive equations are solved to obtain the mid-plane strains. The individual off-axis and material-axis ply stresses at any point in each ply are evaluated from the strain and curvature

values as follows:

$$\mathbf{s} = \bar{\mathbf{Q}}\,\boldsymbol{\varepsilon}^0 + z\,\bar{\mathbf{Q}}\,\mathbf{k}, \tag{3}$$

$$\boldsymbol{\sigma} = \mathbf{T}\,\mathbf{s}, \tag{4}$$

where the positive direction of the z-axis is as shown in Figure 3.

Failure Analysis

Material failure occurs in a composite cylindrical shell if the longitudinal, transverse, or in-plane shear stress of a ply in the shell wall exceeds its strength. Therefore, to avoid this problem, the individual ply stresses must be constrained. The interaction failure criterion presented by Tsai and Wu [24] is used in this research. The Tsai-Wu failure criterion is chosen due to a number of reasons. First, it is widely used and accepted by industry for composite design and analysis. Second, it accounts for the difference in composite material's unequal tensile and compressive failure strengths. Third, it incorporates the interaction between lamina stresses. Finally, it allows a more comprehensive formulation of a design constraint in the optimization problem, since all three lamina stresses are combined into one equation. The general form of this relation, for a plane stress condition, is as follows:

$$\left(\frac{1}{\sigma_{1\mathrm{T}}} - \frac{1}{\sigma_{1\mathrm{C}}}\right)\sigma_1 + \left(\frac{1}{\sigma_{2\mathrm{T}}} - \frac{1}{\sigma_{2\mathrm{C}}}\right)\sigma_2 + \frac{\sigma_1^2}{\sigma_{1\mathrm{T}}\,\sigma_{1\mathrm{C}}} - \frac{\sigma_1\,\sigma_2}{\sqrt{\sigma_{1\mathrm{T}}\,\sigma_{1\mathrm{C}}\,\sigma_{2\mathrm{T}}\,\sigma_{2\mathrm{C}}}} + \frac{\sigma_2^2}{\sigma_{2\mathrm{T}}\,\sigma_{2\mathrm{C}}} + \frac{\sigma_{12}^2}{\sigma_{12\mathrm{S}}^2} < 1. \tag{5}$$

Material-axis ply stresses along with their respective strengths are used in this relation. A value of less than one indicates a safe ply stress configuration.

Buckling and Postbuckling Analysis

The critical buckling load and postbuckling curves shown in Figure 1 are evaluated in this research using analytical formulations. The critical buckling load represents the value of the axial load, which is a minimum with respect to variations in shell buckling modes and is derived using a Donnell-type linear stability analysis [25]. To develop a general relation to predict the buckling load of an axially compressed composite cylindrical shell, the set of Donnell-type stability differential equations are employed as follows:

$$\frac{\partial N_x}{\partial x} + \frac{\partial N_{xy}}{\partial y} = 0, \tag{6}$$

$$\frac{\partial N_{xy}}{\partial x} + \frac{\partial N_y}{\partial y} = 0, \tag{7}$$

$$\frac{\partial^2 M_x}{\partial x^2} + 2\frac{\partial^2 M_{xy}}{\partial x \partial y} + \frac{\partial^2 M_y}{\partial y^2} + \frac{N_y}{R} - \bar{N}_x \frac{\partial^2 w}{\partial x^2} = 0, \tag{8}$$

where $\bar{N}_x$ is the axial stability load that is being computed. The strain-displacement relations for the components of the mid-plane strain and curvature vectors in equations (1) and (2) are written as follows:

$$\varepsilon_x^0 = \frac{\partial u^0}{\partial x}, \tag{9}$$

$$\varepsilon_y^0 = \frac{\partial v^0}{\partial y} - \frac{w}{R}, \tag{10}$$

$$\gamma_{xy}^0 = \frac{\partial u^0}{\partial y} + \frac{\partial v^0}{\partial x}, \tag{11}$$

$$k_x = \frac{\partial^2 w}{\partial x^2}, \tag{12}$$

$$k_y = \frac{\partial^2 w}{\partial y^2}, \tag{13}$$

$$k_{xy} = -2\,\frac{\partial^2 w}{\partial x \partial y}, \tag{14}$$

where u^0 and v^0 are the axial and circumferential displacements of the shell mid-plane, w is the radial displacement of the shell wall, and R is the radius of the shell. Substituting eqs. (1), (2), and (9)–(14) into equations (6)–(8), the necessary set of governing differential equations for the buckling of a cylindrical shell are expressed in terms of displacements of the middle surface of the wall.

To find a solution to the stability differential equations for the following simply supported edge boundary conditions:

$$\text{at} \quad x = 0 \text{ and } L; \qquad N_x = v^0 = w = M_x = 0, \tag{15}$$

a Navier type solution procedure is employed. This involves the use of assumed mid-plane displacement functions in the form of a double Fourier series:

$$u^0 = \bar{u} \cos\left(\frac{m\pi x}{L}\right) \sin\left(\frac{ny}{R}\right), \tag{16}$$

$$v^0 = \bar{v} \sin\left(\frac{m\pi x}{L}\right) \cos\left(\frac{ny}{R}\right), \tag{17}$$

$$w = \bar{w} \sin\left(\frac{m\pi x}{L}\right) \sin\left(\frac{ny}{R}\right), \tag{18}$$

where $\bar{u}$, $\bar{v}$, and $\bar{w}$ represent the unknown amplitudes of the buckling displacements. By appropriately differentiating and substituting equations (16)–(18) into the displacement differential equations, a set of three linear homogeneous algebraic equations, in terms of the unknown displacement amplitudes, is obtained. To obtain a nontrivial solution to these three linear equations, the determinant of the coefficients of $\bar{u}$, $\bar{v}$, and $\bar{w}$ is set equal to zero. Solving for $\bar{N}_x$ leads to the following stability criterion for an axially compressed composite cylindrical shell made of symmetric laminates:

$$\frac{N_x L^2}{\pi^2 D_{11}} = m^2 \left(1 + 2\frac{D_{12} + 2D_{66}}{D_{11}}\beta^2 + \frac{D_{22}}{D_{11}}\beta^4\right) + \frac{L^4}{\pi^4 m^2 D_{11} R^2} \frac{A_{11}A_{22} - A_{12}^2}{A_{11} + \left(\frac{A_{11}A_{22} - A_{12}^2}{A_{66}} - 2A_{12}\right)\beta^2 + A_{22}\beta^4}, \tag{19}$$

where

$$\beta = \frac{nL}{\pi R m}. \tag{20}$$

The critical buckling load, $N_{x_{cr}}$, is obtained by varying m and n (the number of buckle half-waves and waves in the axial and circumferential directions, respectively) until a combination is found that produces the lowest load, $\bar{N}_x$.

The above stability relation is developed under the premise that simply supported edge conditions exist. However, according to Donnell and Wan [26], it has been shown that for cylindrical shells of modest length (greater than 3/4 of a diameter and shorter than 10 or 20 diameters), the end conditions have negligible effects on the buckling load. It is equally important to note that due to the presence of the curvature term (N_y/R) in the third governing differential equation (8), the displacement differential equations are always coupled for both symmetric and unsymmetric laminates. This is in contrast to the results of the stability analysis for composite plates where the differential equations decouple for symmetric laminates and the resulting stability equation is then based solely upon the values of bending stiffness. The differential equations for a flat plate is recovered by allowing $R \to \infty$ in equation (8).

To study the postbuckling behavior of cylindrical shells, the appropriate strain-displacement relations need to be utilized. For nonlinear large deflection theory, the curvatures of the laminate are defined by equations (12)–(14), however, the mid-plane strains (equations (9)–(11)) are now

expressed in terms of second order displacement quantities. The application of this nonlinear theory assumes that the shell wall remains elastic and continuous during the postbuckling process.

The constitutive relations for the composite shell are represented by equations (1) and (2). The differential equations of equilibrium are defined by equations (6)–(8), which are solved using Airy's stress function [26]. This results in two nonlinear partial differential equations, in terms of only the radial wall deflection w and stress function ϕ, that govern the postbuckling behavior of composite cylindrical shells. An exact solution to these two equations is difficult to obtain. Therefore, an approximate solution procedure is used along with the condition of minimum potential energy. The extensional strain energy and the flexural strain energy are written as follows:

$$U_1 = \frac{1}{2}\int_0^L \int_0^{2\pi R} \mathbf{N}^\top \mathbf{a}\, \mathbf{N}\, dx\, dy, \tag{21}$$

$$U_2 = \frac{1}{2}\int_0^L \int_0^{2\pi R} \mathbf{k}^\top \mathbf{d}\, \mathbf{k}\, dx\, dy, \tag{22}$$

where $\mathbf{N}$ is the resultant force vector, $\mathbf{k}$ is the laminate curvature vector, and $\mathbf{a}$ and $\mathbf{d}$ are the compliance matrices. The potential of the externally applied load is defined as follows:

$$U_3 = -\int_0^{2\pi R} \mathbf{N}_x\Big|_{x=L} dy \int_0^L \frac{\partial u}{\partial x}\, dx. \tag{23}$$

Combining equations (21)–(23), the total potential energy function of the system can be expressed as follows:

$$\Pi = U_1 + U_2 + U_3. \tag{24}$$

An approximate radial deflection function must be chosen before evaluating the total potential energy of the system. A Rayleigh-Ritz type solution procedure is used here, and the displacement function is represented by a double Fourier series. The form proposed by Almroth [27] is used in this investigation. It retains five terms in the series solution and has been shown to be in good agreement with experimental data. The function is described as follows:

$$w = w_0 + w_1 \cos\frac{\pi x}{l_x}\cos\frac{\pi y}{l_y} + w_2 \cos\frac{2\pi x}{l_x} + w_3 \cos\frac{2\pi x}{l_x}\cos\frac{2\pi y}{l_y} + w_4 \cos\frac{4\pi x}{l_x}, \tag{25}$$

where $l_x = L/m$ and $l_y = \pi R/n$ are the axial and circumferential half-wavelengths, and w_0 through w_4 are the unknown deflection coefficients. It should be noted that this deflection function does not satisfy clamped or simply supported boundary conditions. However, when a shell is of sufficient length, the edge conditions have negligible effect on buckling [26]. All shells analyzed in this investigation fall into this category.

The above deflection function used along with the compatibility equation results in the Airy stress function ϕ. And further, substitution of w and ϕ into equation (24), along with the evaluation of the necessary integrals, produces a relation for the total potential energy of the system [28], which is a function of the applied axial load on the shell. For a system in equilibrium, the total potential energy of the system must be stationary for any small and arbitrary variation in radial deflection parameters, w_1, w_2, w_3, w_4, and wavelength ratio parameter, μ, since it is considered continuous. It can be shown that the uniform radial deflection parameter w_0 is not independent and, therefore, does not influence the postbuckling problem at all. This requirement translates into the solution of a set of five simultaneous nonlinear equations:

$$\frac{\partial \Pi}{\partial w_1} = \frac{\partial \Pi}{\partial w_2} = \frac{\partial \Pi}{\partial w_3} = \frac{\partial \Pi}{\partial w_4} = \frac{\partial \Pi}{\partial w_\mu} = 0. \tag{26}$$

The actual average end shortening of the cylindrical shell is expressed as follows:

$$\bar{\varepsilon} = -\frac{1}{L}\int_0^L \frac{\partial u^0}{\partial x}\, dx, \tag{27}$$

where $\bar{\varepsilon}$ contains periodic and nonperiodic terms. The nonperiodic terms are the only ones of importance and they lead to the following postbuckling relation for end shortening, in terms of deflection parameters (w_i) and the actual compressive load ($\bar{\sigma}$), as follows:

$$\bar{\varepsilon} = a_{11}\,\bar{\sigma} + \frac{1}{8}\left(w_1^2 + 8w_2^2 + 4w_3^2 + 32\,w_4^2\right)\frac{\pi^2}{l_x^2}. \tag{28}$$

To evaluate the postbuckling behavior of a cylindrical shell, the solutions for w_i and μ are obtained for various values of load parameter $\bar{\sigma}$. The sets of solution values, along with each load parameter, are used to evaluate the end shortening ($\bar{\varepsilon}$) and define equilibrium points along curve AC of Figure 1. However, due to the inconvenience of having the load parameter as an independent variable, an alternative solution formulation is employed by expressing the potential energy in terms of end shortening. This is done by replacing the load parameter in the potential energy relation with the expression for end shortening (equation (28)). Differentiating the new potential energy relation with respect to the problem variables produces five simultaneous nonlinear equations that are now expressed in terms of w_i, μ, and $\bar{\varepsilon}$. These equations are solved for w_i and μ for values of $\bar{\varepsilon}$. However, μ appears in these five equations in a very complicated manner, so a more convenient solution procedure is used by assuming values of μ and solving for w_i and $\bar{\varepsilon}$. Since the value of μ is zero at the critical buckling load (point A, Figure 1) and becomes larger with increased buckling, it is incremented in small steps from zero, and equation (26) is solved for w_i and $\bar{\varepsilon}$ at each incremental value. These solutions also correspond to equilibrium points along curve AC of Figure 1. This procedure is continued until $\bar{\varepsilon}$ reaches a specified maximum value. When enough sets of w_i and $\bar{\varepsilon}$ are known, equation (28) is used to evaluate the corresponding $\bar{\varepsilon}$ and $\bar{\sigma}$ to create a postbuckling curve similar in nature to curve AC.

The energy absorption of a composite cylindrical shell is evaluated by numerically integrating the area under the pre- and postbuckling stress-strain curves and dividing this quantity by the density of the composite. This produces a value called specific energy absorption, which is a measure of effectiveness of energy absorbed. It must be noted, however, that to actually produce a curve like that of AC in Figure 1, the platens of a test machine would need to be separated after initial buckling. Under constant compression, the shell transforms into a new minimum energy postbuckling equilibrium state very rapidly, so it is unrealistic to consider separation of the platens. As a result, the shell drops to the equilibrium state denoted by point B on Figure 1. The portion of the postbuckling curve denoted by AB is referred to as the unstable postbuckling region, and the portion of the curve denoted by BC is referred to as the stable postbuckling region. The unstable postbuckling region is not considered in this investigation. Therefore, only the area under curves OA and BC is numerically integrated in the evaluation of the energy absorption of a shell.

Optimization Formulation

The objective of this investigation is to maximize the energy absorption capability of axially compressed composite cylindrical shells. Constraints are placed upon the material-axis ply stresses, σ_1, σ_2, σ_{12}, at the critical buckling load. The Tsai-Wu interaction failure criterion is used to constrain the stresses in each ply. A constraint is additionally placed upon the critical buckling load to control its value and prevent it from becoming too high. The shell mean radius R and ply orientations θ_i, $i = 1, \ldots, n$, are used as design variables. Upper bounds are imposed on the stresses based upon the failure strength of the particular composite material used for

the shell. The upper limit of the buckling load is based upon information obtained in previous research.

In a standard optimization formulation, the problem is that of minimizing an objective function where the objective is typically some positive quantity such as weight or area. Since the problem addressed in this research is to maximize energy absorption, the objective function is defined as the negative of the the area under the load-deflection curve. This allows application of minimization techniques to produce a maximum. The optimization problem can be mathematically stated as follows:

Minimize:

$$-F(\phi_i), \qquad i = 1, \ldots, \text{NDV}, \qquad \text{(objective function)}$$

where F is the area under the load-deflection curves OA and BC (Figure 1), subject to:

$$g_j(\phi_i) \leq 0, \qquad j = 1, \ldots, \text{NCON}, \qquad \text{(constraints)},$$
$$\phi_{i\text{L}} \leq \phi_i \leq \phi_{i\text{U}}, \qquad \text{(side constraints)},$$

where ϕ is the design variable vector, NDV is the number of design variables, NCON is the total number of constraints, and subscripts L and U refer to lower and upper bounds imposed on the design variables. The side constraints are imposed on the design variables to avoid unrealistic designs. Note that the values of NDV and NCON are different for shells with different wall thicknesses. Since shells with only symmetric laminates are investigated in this study, the number of ply orientations are reduced by a half due to symmetry. Likewise, a Tsai-Wu failure constraint is only applied on stresses in half the plies.

Optimization Procedure

The optimization process is initiated by defining all the necessary preassigned parameters (e.g., shell length and wall thickness) for the problem. Next, the design variables are initialized and the structural analysis is performed. The structural analysis consists of the calculation of all the necessary laminate constitutive properties. The objective function (the numerically integrated area under the force deflection curve) and constraints, which involve calculation of the material-axis ply stresses, are then evaluated followed by a sensitivity analysis. The optimizer consists of a non-linear programming procedure based on the method of feasible directions, as implemented in the computer-code CONMIN [29], along with a two-point exponential approximation method [30]. The two-point method employs an exponential function, which utilizes previous analytical information, in a first-order Taylor-series type relation. The exponent acts as a "goodness of fit parameter" to help determine an approximation that most appropriately adheres to the design data. The approximate analysis procedure is used to reduce the computational costs associated with several evaluations of the objective function and constraints necessary within CONMIN. To reduce possible errors in the approximations, move limits, defined as the maximum fractional change of a design variable value, are imposed as upper and lower bounds on the design variables, ϕ_i. Convergence is based upon the objective function value over three consecutive cycles, where a cycle comprises a complete analysis and optimization. A convergence tolerance of 0.005 is used.

RESULTS

Results obtained using the above optimization procedure are presented in this section. The results of the optimization are compared against a reference (baseline) design. The material and number of plies are varied to investigate their sensitivity to the energy absorption. A total of 15 cylindrical shells are analyzed which include 5 shells of Graphite/Epoxy, Glass/Epoxy, and

Kevlar/Epoxy with 2, 4, 6, 8, and 10 ply symmetric orthotropic laminates, respectively. Optimum configurations for maximum energy absorption are obtained within 3–12 cycles in each case. A variable move limit procedure is employed, during optimization, in which a larger move limit is used initially to accelerate the process, and a tighter limit is used as the optimizer approaches a minimum. Move limits of the order of 0.1–0.01 are used.

The results of the optimization for the cylindrical shells made of symmetric orthotropic laminates are summarized in Table 2 and Figures 4–6. Each of the cylindrical shells are subjected to a compressive strain of 10%. In addition to the stress constraints, a constraint is placed upon the critical buckling load. This constraint is necessary to control the magnitude of the critical buckling load and prevent it from becoming too high. Based upon the maximum critical buckling load information obtained from previous research [31,32], upper bounds are imposed such that the buckling loads remain 10% lower in magnitude than their corresponding optimum values. Table 2 presents the critical buckling load, minimum stable postbuckling load (point B, Figure 1), and specific energy absorption capability of both the reference and the optimum shells. It also lists the ratio of the minimum stable postbuckling load to the classical buckling load. The table indicates that Gr/Ep shells are able to absorb the maximum energy and display the highest buckling loads in both the reference and the optimum shells, followed by the Gl/Ep and the K/Ep shells. This trend is in accordance with results displayed by Farley [6]. The values of the critical buckling loads are all close to or equal to the upper bounds imposed on them (i.e., the constraints are nearly critical). This is due to the fact that one way to increase the area under the load-deflection curve is by increasing the critical buckling load. The optimization procedure, therefore, is greatly influenced by the load limiting constraint, and convergence is reached after this constraint becomes active. The ratios of the minimum stable postbuckling load to the critical buckling load for the reference and optimum cylindrical shells display an expected trend. The minimum stable postbuckling loads exhibit a mean value of approximately 18% of their respective critical buckling load's magnitude. This is in good agreement with the results obtained by Almroth [27], in which the same radial deflection function was used. Previous experimental evidence also shows the value of this ratio to be in the neighborhood of actual test results [33]. Another interesting trend is also observed about this ratio. It is seen that for each group of shells made of the same material, the value of the ratio is highest for the 2- and the 10-ply cases. The smallest value occurs in the 6-ply case for all reference shells and in the 4-ply case for all optimum shells. No conclusion can be drawn at this point about this nonlinear trend.

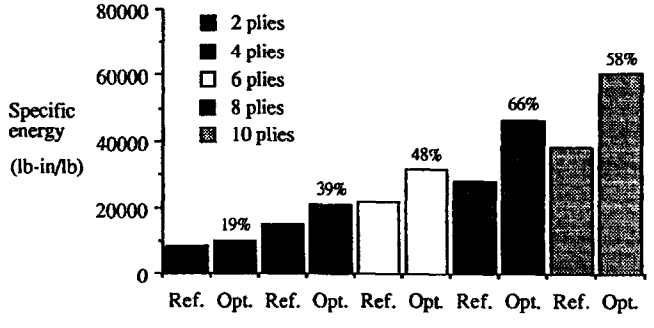

Figure 4. Comparison of energy absorption for Gr/Ep cylindrical shells.

The percent increase in specific energy absorption of the shells, from reference to optimum, are presented in Figures 4–6. Figure 4 shows an improvement in the energy absorption capability for Gr/Ep shells. The maximum increase (66%) occurs in the 8-ply shell, and the 2-ply shell has the lowest overall increase (19%). Similarly, the K/Ep shells display a maximum and a minimum increase of 60% and 23%, respectively, in the 8- and the 2-ply cases (Figure 5). The overall increase in energy absorption are the lowest for the Gl/Ep shells. In this case, the 6-ply shell shows the maximum increase in buckling load (37%) and the 2-ply shell once again yields the

Table 2. Energy absorption and buckling loads of the reference and optimum cylindrical shells.

	No. of Plies	Reference				Optimum			
		$N_{x_{cr}}$ (lb/in)	$N_{x_{min}}$ (lb/in)	$\frac{N_{x_{min}}}{N_{x_{cr}}}$	Energy (lb-in/lb)	$N_{x_{cr}}$ (lb/in)	$N_{x_{min}}$ (lb/in)	$\frac{N_{x_{min}}}{N_{x_{cr}}}$	Energy (lb-in/lb)
Gr/Ep	2	118.1	22.7	0.192	8285.3	152.2	27.1	0.178	9876.2
	4	479.7	90.2	0.188	14909.1	1086.3	160.7	0.148	20681.3
	6	1155.5	203.5	0.176	21575.8	2415.2	372.1	0.154	31848.4
	8	1961.6	383.1	0.195	28090.9	4292.3	755.4	0.176	46727.2
	10	3128.5	638.2	0.204	38345.4	6450.6	1257.8	0.195	60712.7
Gl/Ep	2	94.9	18.2	0.192	4803.2	122.2	21.7	0.178	5699.5
	4	385.6	64.9	0.168	10035.7	520.3	83.2	0.160	12571.4
	6	839.8	140.9	0.167	12238.1	1271.1	230.3	0.181	16738.1
	8	1549.4	268.6	0.173	15500.3	2191.4	385.6	0.176	19714.3
	10	2447.4	428.1	0.174	18085.7	3386.7	612.9	0.181	24014.3
K/Ep	2	52.0	10.3	0.198	4424.5	70.4	13.6	0.193	5465.3
	4	211.9	40.7	0.192	6850.3	508.7	73.7	0.145	9350.2
	6	496.8	93.9	0.189	10166.7	1157.1	180.8	0.156	15933.3
	8	860.9	170.1	0.197	13675.5	1914.2	344.2	0.180	21925.3
	10	1395.3	276.1	0.198	16160.2	2726.2	556.1	0.204	24040.5

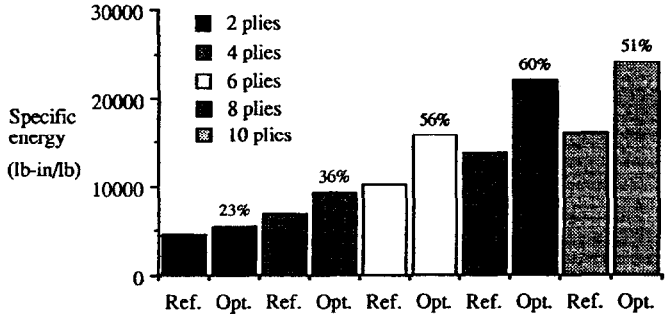

Figure 5. Comparison of energy absorption for K/Ep cylindrical shells.

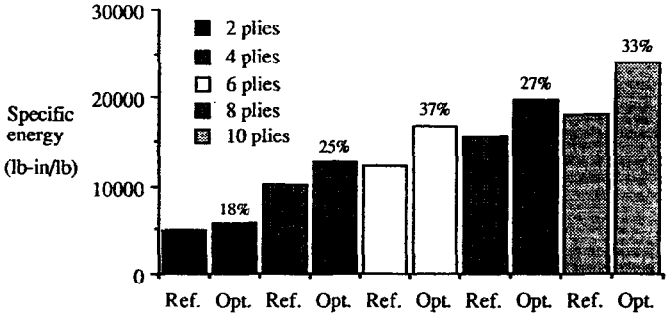

Figure 6. Comparison of energy absorption for Gl/Ep cylindrical shells.

lowest increase (18%), as shown in Figure 6. Since a global minimum cannot be guaranteed in most nonlinear optimization problems, such as these, no conclusion is drawn regarding this nonlinear change of optimum energy absorption with changes in the number of plies, due to possible convergence to a local minimum. The energy absorption capability of both the reference and the optimum shells increase, with the number of plies, almost linearly. This is expected since the wall thickness plays a direct role in supporting the loads and in determining the amount of energy the shell can absorb.

Tables 3–5 present the design variable values for the reference and the optimum shells. The shell radius is allowed to change by ±25% and the plies are allowed to vary between ±90° during optimization. Only half of the ply orientations (θ_i) are presented, due to the conditions of symmetry. From each of these tables, some interesting trends can be observed regarding the radius and the ply orientations. For all 15 cylindrical shells, the radii decrease from their initial value of 10 in found in the reference shells, to a value of 7.5 in (design variable lower bound) found in the optimum shells for all three materials. This increases the slenderness ratio (L/R) and reduces the shell diameter to wall thickness ratio (D/t), and suggests that an increase in the energy absorption capability is also attributed to changes in these ratios. Farley [8] and Sen *et al.* [34] have shown experimentally that a decrease in the ratio D/t is associated with increased energy absorption. It is also interesting to note that although the decrease in the radius reduces the circumferential area, the buckling load (which is directly proportional to circumferential area) and the energy absorption increase for all shells. This suggests that the ply orientations play a major role in energy absorption, as shown by Farley [2]. It must be noted that the radius and, thus, the surface area decrease, thereby reducing the weight of the shell, without weight being used as a constraint. The optimum shells, therefore, support higher buckling loads and absorb more energy while being lighter than the respective reference shells. Tables 3–5 also indicate that the ply angles closer to the mid-plane of the shell wall decrease in magnitude (from their reference value) and those nearer the outer surface increase in magnitude. This trend is due to the fact that the Tsai-Wu constraint criterion is more satisfied by the stress configurations that result from these ply orientations.

Table 3. Comparison of design variables for Gr/Ep shells.

	Reference	Optimum				
		10 plies	8 plies	6 plies	4 plies	2 plies
Mean radius (in)	10.0	7.5	7.5	7.5	7.5	7.5
θ_1 (degrees)	30.0	52.4	51.3	47.8	51.0	39.9
θ_2 (degrees)	−30.0	−26.7	−51.3	−14.3	−16.6	–
θ_3 (degrees)	30.0	16.8	17.1	14.3	–	–
θ_4 (degrees)	−30.0	−16.6	−17.1	–	–	–
θ_5 (degrees)	30.0	16.3	–	–	–	–

Table 4. Comparison of design variables for K/Ep shells.

	Reference	Optimum				
		10 plies	8 plies	6 plies	4 plies	2 plies
Mean radius (in)	10.0	7.5	7.5	7.5	7.5	7.5
θ_1 (degrees)	30.0	45.7	42.4	47.7	48.6	26.8
θ_2 (degrees)	−30.0	−25.4	−21.1	−15.3	−14.2	–
θ_3 (degrees)	30.0	19.3	10.6	14.8	–	–
θ_4 (degrees)	−30.0	−17.4	−9.4	–	–	–
θ_5 (degrees)	30.0	10.3	–	–	–	–

The individual ply stress results of the reference and optimum Gr/Ep cylindrical shells are presented in Table 6. The longitudinal, transverse, and in-plane shear stresses along the material-axis of each ply (σ_1, σ_2, σ_{12}) are constrained using the Tsai-Wu interaction failure criterion. Only half the ply stresses for each shell are shown, due to conditions of symmetry. In this table, the upper bounds on each of these stresses, σ_T and σ_C, represent the material strength in tension and compression, respectively. These bounds are used in the failure criterion in conjunction with

Table 5. Comparison of design variables for Gl/Ep shells.

	Reference	Optimum				
		10 plies	8 plies	6 plies	4 plies	2 plies
Mean radius (in)	10.0	7.5	7.5	7.5	7.5	7.5
θ_1 (degrees)	30.0	41.1	35.2	29.8	53.1	57.6
θ_2 (degrees)	−30.0	−30.8	−21.8	−23.8	−37.1	–
θ_3 (degrees)	30.0	26.5	21.8	15.7	–	–
θ_4 (degrees)	−30.0	−23.3	−20.8	–	–	–
θ_5 (degrees)	30.0	23.4	–	–	–	–

the in-plane ply stresses (equation (5)). The Tsai-Wu criteria predicts a fail-safe design (a value less than 1) when ply stresses are less than their respective bounds. Note that the values of stress in each reference shell change as the wall thicknesses are changed. It is obvious from this table that optimization leads to significant changes in the stress distributions at each ply level. The stresses remain well within the prescribed bounds. However, in some cases the nature of the stresses change from tensile to compressive and vice versa after optimization. For example, in the 10-ply shell at ply 1, σ_2 is tensile in the reference shell and compressive in the optimum shell. The nature of these stresses also varies with changes in the number of plies. For example, at ply 1 of the optimum configuration, σ_1 remains compressive for the 2-, 4-, 6-, and 8-ply arrangements, but becomes tensile in the 10-ply arrangement. Similar trends can be observed in the K/Ep and Gl/Ep shells. The magnitudes of the ply stresses in all three cases vary with the type of material and the number of plies. Although no specific conclusion can be drawn regarding these magnitudes, a general trend in the stresses is observed for all three cases. The normal stress in plies near the wall mid-plane for the optimum shells is higher in magnitude than the normal stress in the plies away from the mid-plane. This is in accordance with a previous observation that the fiber angles of the inner plies tend to decrease in magnitude. As a result, the fibers in these plies are subjected to a larger axial loading, which in turn causes the normal stresses to increase. By examining Table 6, it is also observed that the dominating stresses in the shell walls are the normal and shear stresses. The high values of these stresses can attribute to mechanisms which initiate shell failure.

Figures 7–9 present the iteration histories of the objective functions for each of the shells. The consistent monotonique increases in the objective function values (energy absorption), in all cases, are due to the fact that the initial designs are feasible designs, that is, all constraints are satisfied. Convergence of the optimization problem is very efficient and occurs in relatively few cycles, due to the load limiting constraint.

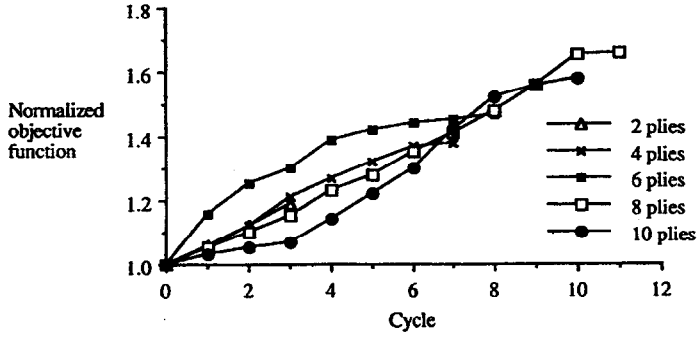

Figure 7. Objective function iteration histories for Gr/Ep cylindrical shells.

Table 6. Material-axis stresses in reference and optimum Gr/Ep shells.

		Bounds (ksi)		10 plies		8 plies		6 plies		4 plies		2 plies	
		σ_T	σ_C	Ref.	Opt.	Ref.	Opt.	Ref.	Opt.	Ref.	Opt.	Ref.	Opt.
1†	σ_1	210.0	−210.0	−29.7	7.0	−26.6	−5.2	−17.0	−3.5	−13.0	−12.7	−4.4	−4.5
	σ_2	7.5	−30.0	2.4	−2.0	2.1	−3.0	1.3	−1.7	1.0	0.2	−1.5	−3.1
	σ_{12}	14.0	−14.0	7.8	9.2	5.9	9.0	4.9	5.3	2.9	6.8	2.6	3.7
2†	σ_1	210.0	−210.0	−40.0	−64.4	−26.6	−5.2	−28.2	−60.9	−13.0	−43.4		
	σ_2	7.5	−30.0	2.9	1.4	2.1	−3.0	1.8	1.2	1.0	1.6		
	σ_{12}	14.0	−14.0	−7.2	−7.8	−5.9	−9.0	−4.3	−2.2	−2.9	−5.5		
3†	σ_1	210.0	−210.0	−29.7	−91.9	−26.6	−100.5	−17.0	−57.1				
	σ_2	7.5	−30.0	2.4	2.6	2.1	1.4	1.3	1.0				
	σ_{12}	14.0	−14.0	7.8	4.8	5.9	5.2	4.9	2.9				
4†	σ_1	210.0	−210.0	−40.0	−87.7	−26.6	−100.5						
	σ_2	7.5	−30.0	2.9	2.4	2.1	1.4						
	σ_{12}	14.0	−14.0	−7.2	−5.5	−5.9	−5.2						
5†	σ_1	210.0	−210.0	−29.7	−92.7								
	σ_2	7.5	−30.0	2.4	2.7								
	σ_{12}	14.0	−14.0	7.8	4.7								

†Ply number.

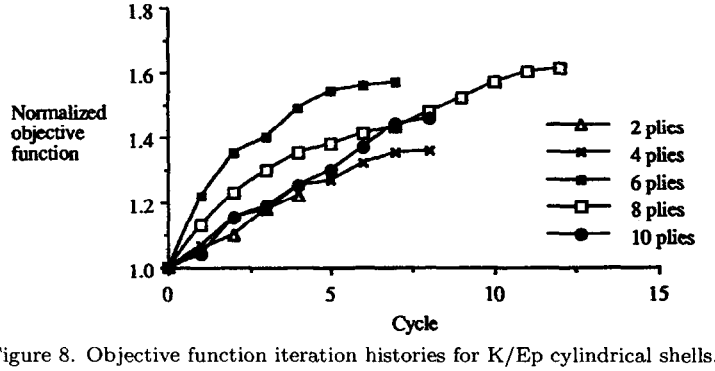

Figure 8. Objective function iteration histories for K/Ep cylindrical shells.

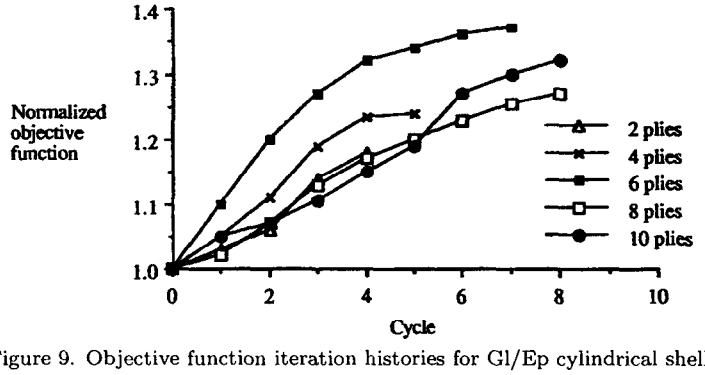

Figure 9. Objective function iteration histories for Gl/Ep cylindrical shells.

CONCLUSIONS

In this research, the optimum design of composite cylindrical shells, under axial compressive loading, is addressed for maximizing the energy absorbing capability of the shells. A sensitivity analysis is performed to study the effect of total number of plies and material constituent properties on the buckling load. The radius of the shell and ply orientations are used as design

variables. Constraints are imposed on the longitudinal, transverse, and shear in-plane ply stresses and on the critical buckling load. The optimization is performed using the method of feasible directions. A two-point exponential approximation method is used to reduce the computational effort. Results are presented for shells made of Gr/Ep, Gl/Ep, and K/Ep orthotropic laminates with five different wall thicknesses. The procedure yields improvements in the energy absorbing capabilities for all shells. Optimum energy absorption configurations are obtained within 3–12 cycles. The following observations are made from this study:

(1) Optimization increased the energy absorbing capability, from the reference values, for all the composite cylindrical shells. Gr/Ep and K/Ep yielded the highest percent increases.
(2) Gr/Ep shells absorbed the most energy followed by K/Ep and Gl/Ep, respectively. These results agree with experimentally observed data.
(3) The ratio of the minimum stable postbuckling load to the critical buckling load agreed well with previous analytical and experimental work.
(4) Significant changes occured in the values of the design variables. Ply orientations nearer the wall mid-plane decreased in magnitude and those farther away increased in magnitude. The radius reduced, thereby increasing the slenderness ratio, indicating that shells of smaller radii are more efficient for energy absorption.
(5) Reductions were obtained in the shell weights, although weight was not used as a constraint in the optimization formulation.
(6) The magnitudes and the nature of the stresses in each ply changed significantly, from reference to optimum, and with changes in wall thicknesses. Gr/Ep and K/Ep displayed the most significant changes.
(7) Convergence was governed by the load limiting constraint imposed on the critical buckling load.

REFERENCES

1. G.L. Farley, A method of predicting the energy-absorption capability of composite subfloor beams, *Journal of the American Helicopter Society* **34**, 63–67 (1989).
2. G.L. Farley, Energy absorption capability of composite tubes and beams, Ph.D. Dissertation, Virginia Polytechnic Institute and State University, Blacksburg, VA, (1989).
3. W. Zhou, J.I. Craig and S.V. Hanagud, Crashworthy behavior of graphite epoxy sine wave webs, *Proc. 32nd AIAA/ASME/ASCE/AHS/ASC Structures, Structural Dynamics and Materials Conference*, Baltimore, MD, April 1991, pp. 1618–1626, (1991).
4. M.J. Czaplicki, R.E. Robertson and P.H. Thornton, Comparison of bevel and tulip triggered pultruded tubes for energy absorption, *Composites Science and Technology* **40**, 31–46 (1991).
5. A.H. Fairfull and D. Hull, Effects of specimen dimensions on the specific energy absorption of fibre composite tubes, *Proc. ICCM-VI and ECCM2*, London, July 1987, (Edited by F.L. Matthews, N.C.R. Buskell, J.M. Hodgkinson and J. Morton), pp. 336–345, Elsevier, (1987).
6. G.L. Farley, Energy absorption of composite materials, *Journal of Composite Materials* **17**, 267–279 (1983).
7. G.L. Farley, Effect of fiber and matrix maximum strain on the energy absorption of composite materials, *Journal of Composite Materials* **20**, 322–324 (1986).
8. G.L. Farley, Effect of specimen geometry on the energy absorption capability of composite materials, *Journal of Composite Materials* **20**, 390–400 (1986).
9. G.L. Farley, Energy absorption capability and scalability of square cross section composite tube specimens, *Journal of the American Helicopter Society* **34**, 59–62 (1989).
10. G.L. Farley, R.K. Bird and J.T. Modlin, The role of fiber and matrix on crash energy absorption of composite materials, *Journal of the American Helicopter Society* **34**, 52–58 (1989).
11. G.L. Farley and R.M. Jones, Crushing characteristics of continuous fiber-reinforced composite tubes, *Journal of Composite Materials* **26** (1), 37–50 (1992).
12. G.L. Farley and R.M. Jones, Prediction of the energy-absorption capability of composite tubes, *Journal of Composite Materials* **26** (3), 388–404 (1992).
13. D. Hull, A unified approach to progressive crushing of fibre-reinforced composite tubes, *Composites Science and Technology* **40**, 377–421 (1991).
14. H. Fukunaga and G.N. Vanderplaats, Stiffness optimization of orthotropic laminated composites using lamination parameters, *AIAA Journal* **29** (2), 641–646 (1991).
15. Z. Gurdal and R.T. Haftka, Optimization of composite laminates, *NATO/DFG ASI, Optimization of Large Structural Systems, Lecture Notes*, September 1991, Vol. 1, pp. 200–215, Berchtesgaden, Germany, (1991).

16. J. Onada, Optimal laminate configurations of cylindrical shells for axial buckling, *AIAA Journal* **23** (7), 1093–1098 (1985).
17. P. Pederson, Optimal orientation of anisotropic materials, *NATO/DFG ASI, Optimization of Large Structural Systems, Lecture Notes*, September 1991, Vol. 1, pp. 168–200, Berchtesgaden, Germany, (1991).
18. G.N. Vanderplaats and T.A. Weisshaar, Optimum design of composite structures, *Journal for Numerical Methods in Engineering* **19**, 437–448 (1989).
19. R. Zimmermann, Optimization of axially compressed fiber composite cylindrical shells, *Proc. International Seminar Organized by Deutsche Forschungsanstalt für Luft- und Raumfahrt (DLR)*, Bonn, June 1989, (1989).
20. J.M. Ferreira, A. Chattopadhyay and S.J. Pringnitz, Reducing edge delamination stresses in composite plates using multiobjective optimization, *Proc. 1993 AIAA/AHS/ASEE Aerospace Design Conference*, Anaheim, CA, February 1993, (1993); *Composites Engineering* (to appear).
21. R.V. Lust, Structural optimization with crashworthiness constraints, Presented at the 3^{rd} *Air Force/NASA Symposium On Recent Advances in Multidisciplinary Analysis and Optimization*, San Francisco, CA, September 1990, (1990).
22. A.O. Bolukbasi, Crash-resistant rotorcraft preliminary design optimization, *Proc.* 47^{th} *Annual Forum of the American Helicopter Society*, Phoenix, AZ, May 1991, Volume 2, pp. 1237–1248, (1991).
23. J.R. Vinson and R.L. Sierakowski, *The Behavior of Structures Composed of Composite Materials*, Kluwer, Dordrecht, (1987).
24. S.W. Tsai and E.M. Wu, A general theory of strength for anisotropic materials, *Journal of Composite Materials* **5**, 58–80 (1971).
25. R.M. Jones, Buckling of circular cylindrical shells with multiple orthotropic layers and eccentric stiffeners, *AIAA Journal* **6** (12), 2301–2305 (1968).
26. L.H. Donnell and C.C. Wan, Effect of imperfections on buckling of thin cylinders and columns under axial compression, *Journal of Applied Mechanics* **17** (1), 73–83 (1950).
27. B.O. Almroth, Postbuckling behavior of axially compressed circular cylinders, *AIAA Journal* **1** (3), 630–633 (1963).
28. N.S. Khot, Buckling and postbuckling behavior of composite cylindrical shells under axial compression, *AIAA Journal* **8** (2), 229–235 (1970).
29. G.N. Vanderplaats, *CONMIN—A Program for Constrained Function Minimization*, User's Manual, NASA TMX-62282, (1973).
30. G.M. Fadel, M.F. Riley and J.F. Barthelemy, Two-point exponential approximation method for structural optimization, *Structural Optimization* **2**, 117–124 (1990).
31. A. Chattopadhyay and J.M. Ferreira, Design sensitivity and optimization of composite cylinders, *Composites Engineering* **3** (2), 169–179 (1992).
32. J.M. Ferreira, Structural optimization and design sensitivity of composite cylindrical shells for buckling and postbuckling, M.S. Thesis, Arizona State University, (1992).
33. W. Thielemann, New developments in the nonlinear theories of buckling of thin cylindrical shells, *Proc. Durand Centennial Conference*, pp. 76–119, Pergamon Press, (1960).
34. J.K. Sen and C.C. Dremann, Design development tests for composite crashworthy helicopter fuselage, *SAMPE Quarterly* **17** (1), 29–39 (1985).